(4)

AD-A196 010

DTIC FILE COPY

REPORT DOCUMENTATION PAGE

DTIC ELECTE JUL 25 1988 S D H

Unclassified	1b RESTRICTIVE MARKINGS
2a. SECURITY CLASSIFICATION AUTHORITY	3. DISTRIBUTION / AVAILABILITY OF REPORT Approved for public release and sale. Distribution unlimited.
2b. DECLASSIFICATION / DOWNGRADING SCHEDULE	
4. PERFORMING ORGANIZATION REPORT NUMBER(S) ONR Technical Report No. 2	5. MONITORING ORGANIZATION REPORT NUMBER(S)
6a. NAME OF PERFORMING ORGANIZATION UNIVERSITY OF WYOMING	6b. OFFICE SYMBOL (If applicable)
6c. ADDRESS (City, State, and ZIP Code) DEPARTMENT OF CHEMISTRY UNIVERSITY OF WYOMING LARAMIE WY 82071-3838	7a. NAME OF MONITORING ORGANIZATION Office of Naval Research Resident Representative 7b. ADDRESS (City, State, and ZIP Code) University of New Mexico Bandelier Hall West Albuquerque, NM 87131
8a. NAME OF FUNDING / SPONSORING ORGANIZATION Office of Naval Research	8b. OFFICE SYMBOL (If applicable) ONR
8c. ADDRESS (City, State, and ZIP Code) 800 N. Quincy Street Arlington, VA 2217	9. PROCUREMENT INSTRUMENT IDENTIFICATION NUMBER N00014-87-K-0674
	10. SOURCE OF FUNDING NUMBERS PROGRAM ELEMENT NO. / PROJECT NO. / TASK NO. R & T 41330190 / WORK UNIT ACCESSION NO.

11. TITLE (Include Security Classification)
(u) Quartz Microbalance Studies of Deposition and Dissolution Mechanisms of Electrochromic Films of Diheptylviologen Bromide

12. PERSONAL AUTHOR(S)
Gregory S. Ostrom and Daniel A. Buttry*

13a. TYPE OF REPORT	13b. TIME COVERED	14. DATE OF REPORT (Year, Month, Day)	15. PAGE COUNT
Technical	FROM 9/87 TO 6/88	1988 July 6	33

16. SUPPLEMENTARY NOTATION
Prepared for publication in the Journal of Electroanalytical and Interfacial Electrochemistry

17 COSATI CODES		
FIELD	GROUP	SUB-GROUP

18. SUBJECT TERMS (Continue on reverse if necessary and identify by block number)
electrochemistry, quartz crystal microbalance, electrochromism

19. ABSTRACT (Continue on reverse if necessary and identify by block number)

Abstract - The quartz crystal microbalance (QCM) technique is used in conjunction with cyclic voltammetric and potential step measurements to study the deposition and dissolution mechanisms of thin films of diheptylviologen bromide. Deposition of a uniform, compact film with little incorporation of supporting electrolyte is indicated for potential steps well past the first reduction wave of the viologen. Films with considerable surface roughness are deposited when using potential sweep methods, depending on conditions. Methods are presented which provide the apparent molar mass of the depositing species from appropriate combination of the QCM and electrochemical data. The use of microgravimetric Anson plots together with conventional Anson plots provides a particularly useful approach to such determinations. Due to the potentially detrimental influence of non-uniform current density on the QCM measurements, an ancillary study of copper deposition was carried out using the same concentrations and ionic strengths as those in the viologen experiments. This demonstrated the uniformity of the current density in the viologen experiments and verified the use of QCM measurements under such conditions.

20 DISTRIBUTION / AVAILABILITY OF ABSTRACT	21 ABSTRACT SECURITY CLASSIFICATION
☒ UNCLASSIFIED/UNLIMITED ☐ SAME AS RPT ☐ DTIC USERS	Unclassified
22a NAME OF RESPONSIBLE INDIVIDUAL Daniel A. Buttry	22b TELEPHONE (Include Area Code) (307) 766-6677
	22c OFFICE SYMBOL

DD FORM 1473, 84 MAR 83 APR edition may be used until exhausted
All other editions are obsolete

SECURITY CLASSIFICATION OF THIS PAGE

OFFICE OF NAVAL RESEARCH

CONTRACT NUMBER N00014-87-K-0674

R & T CODE 413301901

Technical Report # 2

Quartz Crystal Microbalance Studies of Deposition and Dissolution Mechanisms of Electrochromic Films of Diheptylviologen Bromide

Gregory S. Ostrom and Daniel A. Buttry*
Department of Chemistry
University of Wyoming
Laramie, WY 82071-3838

Prepared for publication in the Journal of Electroanalytical and Interfacial Electrochemistry

July 7, 1988

Quartz Crystal Microbalance Studies of Deposition and Dissolution Mechanisms of Electrochromic Films of Diheptylviologen Bromide

Gregory S. Ostrom and Daniel A. Buttry*
Department of Chemistry
Box 3838
University of Wyoming
Laramie, WY 82071

Abstract - The quartz crystal microbalance (QCM) technique is used in conjunction with cyclic voltammetric and potential step measurements to study the deposition and dissolution mechanisms of thin films of diheptylviologen bromide. Deposition of a uniform, compact film with little incorporation of supporting electrolyte is indicated for potential steps well past the first reduction wave of the viologen. Films with considerable surface roughness are deposited when using potential sweep methods, depending on conditions. Methods are presented which provide the apparent molar mass of the depositing species from appropriate combination of the QCM and electrochemical data. The use of microgravimetric Anson plots together with conventional Anson plots provides a particularly useful approach to such determinations. Due to the potentially detrimental influence of non-uniform current density on the QCM measurements, an ancillary study of copper deposition was carried out using the same concentrations and ionic strengths as those in the viologen experiments. This demonstrated the uniformity of the current density in the viologen experiments and verified the use of QCM measurements under such conditions.

INTRODUCTION

Interest in the use of electrochromic materials in display applications has led to a number of investigations into the electrochemistry of films of the highly colored precipitates formed from the reduction of several different viologen compounds (1-25). Of these, 1,1'-diheptyl-4,4'-bipyridinium dibromide ($HVBr_2$) and other salts of this viologen have been the most extensively studied. A variety of additional techniques have been employed for the study of the films of these compounds, including spectroelectrochemistry (4b, 5, 7-9, 10b, 10d, 15-17, 24b), and ESR (10c), Raman (13, 20-23), photoacoustic (24a,24c), and photothermal (24d) spectroscopies. One of the conclusions which can be drawn from these studies is that the viologens are usually adsorbed on the surface at monolayer or submonolayer coverages prior to their reduction (10-12, 14, 20-23, 25), and that this adsorbed film influences the nucleation and growth of the deposit (25). In addition, the stripping behavior of the deposits seems to depend on the structure of the viologen (3b, 4a, 9a, 9c, 18), the length of time that the deposit is left in its reduced form and the deposition potential (9a, 9c), and the supporting electrolyte (6,17). In a particularly novel approach (13), the use of cyclodextrin to form an inclusion complex with the viologen was shown to inhibit the recrystallization of the film which has been thought to be the cause of the ageing phenomenon (9a, 9c). The general implication of these studies is that the detailed composition of the reduced film (i.e. solvent and supporting electrolyte content), as well as its structure, will have a strong influence on its electrochemical behavior. Of the few methods available for probing the composition of thin films in situ, the quartz crystal microbalance (QCM) provides one of the simplest and most direct approaches to the problem.

Recent work in several research groups (26-28) has demonstrated the utility of QCM technology for the study of surface processes in electrochemical measurements. The QCM is a mass sensitive piezoelectric device (typically employed as a disk-shaped transducer) which oscillates in a mechanically resonant shear mode by application of an alternating, high frequency electric field using electrodes deposited on both sides of the disk. A minute change in the mass of one of the electrodes by virtue of an electrochemical (or other) event causes a detectable change in the resonant frequency which can be used to infer the mass change. The QCM has been used to

study monolayer oxide formation on gold electrodes (28a), underpotential deposition of various metals (27b,c), bulk metal deposition and dissolution (29,30), adsorption and desorption of surfactant derivatives (26c), and ion and solvent transport which are consequences of redox processes in various types of thin polymer films on gold electrodes (26a,b). In addition to these studies in which the QCM has been used to detect mass changes at the electrode surface, it has also been shown that the QCM is sensitive to morphological changes of the electrode surface or films on its surface (29b, 30, 31).

In addition to the uses listed above, the QCM lends itself well to observations of the deposition and stripping of thin organic films on electrodes. The importance of such depositions is demonstrated by their wide application in the electropolymerization of thin layers of redox and electrochemically inert polymers (32). A recent report demonstrates another method for deposition of thin organic films by precipitation from micellar solutions (33). While the methods for deposition of such thin films are fairly well established, the mechanisms of their deposition on and removal from the surface have not been as thoroughly studied. Due to its intrinsic sensitivity to mass changes at electrode surfaces, the QCM represents a powerful tool for such studies.

In this report, the QCM is used to study the deposition and dissolution of thin films of diheptylviologen bromide (HVBr), the precipitate formed by the one electron reduction of HV^{2+} in the presence of bromide ion in aqueous solutions. The electrochemistry of HV2+ is studied under both potential step and potential sweep conditions to gain insight into the mechanisms of deposition and dissolution. Comparison of the QCM data for this system to those for copper deposition from sulfuric acid at identical concentrations and ionic strengths is used to probe the influence of non-uniform current density distributions on the QCM measurement.

EXPERIMENTAL

Materials and Instrumentation. The $HVBr_2$ was either obtained from Aldrich Chemical Company or prepared by reaction of 4,4'-bipyridine and 1-bromoheptane in acetonitrile. Reagent grade chemicals were used throughout, unless otherwise specified. Prior to beginning the experiments, the solutions were deaerated for 20 minutes with Ar which had been passed through a vanadous sulfate oxygen scrubber. Water for the supporting electrolyte solutions was obtained from a Millipore deionizer.

The basic instrumentation for the QCM/electrochemical measurement has been previously described (26,27b). The facility of the data acquisition and analysis has been increased considerably by interfacing the instrument to an IBM PC/AT using a Data Translation DT2801-A data acquisition and control board. This was driven from the ASYST programming environment, which also contains routines for digital smoothing, differentiation, integration, and other types of data manipulation. Backgrounds for potential scans and steps into the region of interest in the absence of $HVBr_2$ were collected and digitally subtracted from those in the presence of the viologen for the precise comparison of frequency and charge data. One inch diameter, overtone polished, 5 MHz AT-cut quartz crystals with both sides parallel (Valpey-Fisher) were coated with a thin Cr adhesion layer (ca. 1.5 to 3.0 nm) followed by a 300 nm thick gold layer. The gold electrode has a keyhole pattern which has been described (28c). The piezoelectrically and electrochemically active areas are 0.28 and 0.34 cm^2, respectively. The electrochemical cell had a conventional H-cell design with a number 9 o-ring joint blown onto the side for mounting the crystal. Thus, only one side of the crystal was exposed to the solution to prevent capacitive shunting of the oscillator circuit (28c). A Pt counter electrode was used, along with a Ag/AgCl reference electrode, to which all potentials are referenced.

Methods. The measurement of mass changes at the electrode surface using the QCM relies on a change in the mechanical resonant frequency of the quartz crystal which is induced by the change in mass. Sauerbrey was the first to show that this effect could be used for the precise determination of mass changes at the QCM surface (34). He proposed the following equation which describes a linear dependence of the frequency change on the mass change.

$$\Delta f = - K \Delta m \qquad (1)$$

Δf is the change in the resonant frequency of the crystal (in Hz) induced by the mass change, Δm is the mass change (in micrograms per square centimeter of surface area) , and K is the proportionality constant which is 56.6 Hz/microgram/cm^2 for a 5 MHz AT-cut crystal. The negative sign indicates a decrease in the crystal resonant frequency with increasing mass. The equation is rigorously valid in the limit of deposition of infinitely thin layers of perfectly elastic materials (35), and is applicable under conditions in which the deposited film is behaving elastically and the total frequency change is not too large (35,36). While it has been clearly shown that the QCM frequency

depends on the density and viscosity of the solution layer near its surface (37) and on the materials properties of the deposited film (37b), the above equation is valid to the extent that the film is uniform, thin, and elastic and the solution component to the signal remains constant during the measurement. Thus, given the proper conditions, electrochemically induced mass changes may be compared quantitatively with electrochemical parameters (e.g. current, charge, etc.).

In comparing QCM frequency changes with electrochemical data it is useful to manipulate the data so as to optimize the comparison. In the present case, since the reduction of $HV2^+$ to HV^+ results in its deposition as HVBr in the presence of bromide ion, one wishes to make quantitative comparisons of the total frequency change and the total charge passed during the reduction. This can be done by recognizing that the current is an instantaneous measure of reactant flux at the electrode surface, while the frequency is an integral measure of the total delivery of reactant to the surface. Thus, as was recently pointed out by Deakin and Melroy for the case of underpotential deposition (27c), the current should be related to the derivative of the frequency with respect to potential (time), and the charge should be directly related to the frequency. These relationships are shown below.

$$i = (d(\Delta f)/dE) (10^{-6} v n F) / (MW_f K) \qquad (2)$$

$$Q = (10^{-6} \Delta f F) / (MW_f K) \qquad (3)$$

The current density (in ampere/cm^2) is given by i, E is the electrode potential (in volts), v is the scan rate (in volts/s), n is the number of electrons transferred to effect the deposition, F is the Faraday constant, MW_f is the apparent molar mass of the species which is being deposited, K is the proportionality constant described in equation 1, and Q is the charge (in coulombs/cm^2). Use of these equations allows for quantitative comparison of the total charge and frequency change (equation 3), and of the current and the instantaneous rate of deposition (equation 2). The derivative representation given in equation 2 is especially well suited for detection of subtle relationships between the current and the instantaneous rate of deposition. Both methods of data representation are used in this work.

RESULTS

Potential Sweep Experiments. The deposition of films of HVBr was studied using cyclic voltammetry (CV) at several scan rates and solution

concentrations of the HV^{2+} ion. Experiments were generally carried out with solutions of 0.3 M KBr, although some other concentrations of supporting electrolyte were investigated. The experiments are done by sweeping the potential in the region of interest and recording the frequency (which is a measure of the cumulative mass change) and the current.

Figure 1 shows the CV/QCM curves for a negative scan to a potential past both reduction peaks of HV^{2+}. The peak for the first reduction process appears in the CV at approximately -0.55 V. This corresponds to reduction of HV^{2+} to a one electron reduced radical form, HV^{+}, and its coincident deposition as the bromide salt. The decrease in the QCM frequency (increase in mass) which begins at this potential clearly shows that the deposition is proceeding. At approximately -0.80 V a second peak is observed in the CV which corresponds to the reduction of the HV^{+} within the film to the neutral form of the viologen, HV. The QCM shows loss of mass in the potential region of this reduction, suggesting expulsion of the bromide anions as electrons are injected into the film. The ratio of the frequency decrease for the first reduction to the frequency increase for the second reduction is roughly 5:1, as is the ratio of the mass of HVBr to that of Br (5.4:1). This is as expected for the deposition and loss of these species for the two redox processes, respectively. A more quantitative comparison of the frequency changes and electrochemical charges is given below.

On the return scan, four peaks are observed at ca. -0.65, -0.51, and -0.35 V, the last being a composite of two neighboring peaks whose relative definition is a strong function of scan rate and solution conditions. The QCM curve shows that the peaks at -0.65 and -0.51 V are associated with a net mass increase (frequency decrease), probably bromide insertion. This indicates that both of these peaks are from HV oxidation to HV^{+}, in agreement with previous workers (3b). The net mass increase for this process is larger than that for the initial reduction of HV^{+} to HV. This is due to the deposition of additional material during the period of the scan between the reduction and subsequent oxidation. The two waves centered at -0.35 V result from an oxidation which causes a mass loss from the electrode surface, implying that these waves correspond to oxidation of HVBr to HV^{2+} with simultaneous film dissolution. After this final oxidation, the frequency returns to its initial value. This implies gross reversibility of the processes responsible for the mass changes. The appearance of the voltammetric features caused by reduction

to the HV state is strongly dependent on many things, including scan rate, concentration of the viologen, and the nature of the supporting electrolyte. These time-dependent, irreversible changes will not be examined further in this communication.

As will be shown below, quantitative comparison of the QCM and electrochemical data is better done by examination of plots of frequency versus charge. For these comparisons we restrict ourselves to examining only the first reduction, i.e. from HV2+ to HV+. A CV scan over only the first wave is shown in Figure 2 along with the QCM curve for this scan. The response is that of a simple diffusion controlled reduction followed by deposition of the product, with subsequent oxidation leading to a stripping peak typical for the removal of precipitates from the electrode (38). Note that the reduction and oxidation processes give only a single peak each at this scan rate, while for scans over both waves all but the first reduction process gave complex, multiple peaked responses. The QCM response reveals mass gain during reduction and mass loss during oxidation. The mass change is completely reversible, in the sense that the initial frequency is regained at the end of the scan.

Recalling that the frequency is an integral measure of the total amount of material which has been deposited (removed) and the charge is an integral measure of the total amount of material which has been reduced (oxidized), one expects the frequency to track the charge. This notion is expressed as equation 3 above. In addition, if reduction induces deposition with 100% efficiency, and if the apparent molar mass of the depositing species (MW_f) remains constant throughout the deposition, then a plot of Δf versus Q should be linear, and its slope should give MW_f directly. Thus, for the present case, linear Δf versus Q plots imply either that the HVBr is deposited in the film with essentially no solvent or supporting electrolyte or that a constant proportion of solvent and/or supporting electrolyte and/or $HVBr_2$ is incorporated into the film during HVBr deposition. These cases should be distinguishable from the slopes of the plots if 100% current efficiency for deposition can be demonstrated from the electrochemical results. The use of such Δf versus Q plots requires an assumption that the film behaves as an elastic layer. It will be shown below that a quantitative comparison of the frequency change and charge passed during a potential step experiment (resulting in diffusion controlled reduction and deposition of the product) verifies the assumption.

Figure 3a shows a plot of Δf versus Q for the scan in Figure 2. Figures 3b and 3c show plots of Δf versus Q for scans done at higher scan rates. These plots show that the coulombic efficiency for the deposition and stripping events is essentially 100% because the cathodic and anodic charges are equal. Relatively linear plots are obtained for the reductive branches of the scans, but a large hysterisis exists between the reductive and oxidative branches. This hysterisis is much larger at high scan rates than at low ones. The slopes of the reductive branches of the plots in Figure 3a, 3b, and 3c give MW_f's of 411 g/mole, 424 g/mole, and 472 g/mole, respectively. Table 1 gives the slopes of such plots for two $HVBr_2$ concentrations and two KBr concentrations at a variety of scan rates. These values should be compared to the molar mass of HVBr, 434.5 g/mole. The data show that at lower scan rates the value of MW_f obtained from the slope approaches the molar mass of HVBr, indicating relatively uniform deposition (31) of a film predominantly composed of HVBr. Increasing scan rate and increasing KBr concentration appear to cause an increase in MW_f. There are a number of possible causes for this behavior.

One possibility is that solvent and/or supporting electrolyte are incorporated into the HVBr film during deposition, and that this incorporation is more probable at higher scan rates due to the more rapid formation of the film. The increased density of the 3 M KBr solution relative to the 0.3 M solution could then be the cause of the increased values of MW_f seen at the higher concentrations. However, it will be shown in a later section that the good agreement of MW_f and the molar mass of HVBr obtained for potential step experiments (in which the film is formed extremely quickly) casts doubt on this model. Another possibility is that $HVBr_2$ is incorporated within the growing film. This seems unlikely, however, due to its relatively high solubility. Also, while it has been shown that $HVBr_2$ forms micelles, and it seems reasonable that aggregates of this type could somehow induce the codeposition of HVBr and $HVBr_2$ (9c), the concentrations of $HVBr_2$ used in the present work are well below the reported critical micelle concentration for $HVBr_2$ of 10 mM (at an ionic strength of 0.1 M)(9a,9c), thereby excluding micelle formation as a mechanism for codeposition.

The favored explanation is that the film surface is not smooth when it is deposited under potential sweep conditions. As noted above, surface roughness causes trapping of the solution within the pockets on the rough surface (31). This would cause anomalously high values of MW_f to be calculated from the Δf

versus Q plots. An increase in the solution density would result in an increase in the frequency change caused by this effect. A plausible cause for nonuniform deposition may be found in the requirement for nucleation sites for film growth. If the number of nucleation sites is not large, then the film deposition will occur as growth of isolated hemispheres and, finally, a merging of these hemispheres together. The extent to which these hemispheres merge together during the CV scan, as well as the initial nucleation site density, should determine the number and size distribution of the pores on the surface, and therefore the extent of solution trapping within these pores. Assuming that the number of nuclei depends both on the applied potential (which, of course, varies during the scan) and on the time spent at a given potential (i.e. progressive nucleation) (11), then only a small number of sites may be created during a rapid scan. This will lead to larger pores and more trapping. At lower scan rates, more sites may be created, leading to smaller pores and less trapping.

One needs also to account for the hysterisis between the anodic and cathodic branches of the Δf versus Q plots. Several scenarios can be put forth for their rationalization. All of these must account for the fact that at high scan rates the passage of anodic charge is not accompanied by sufficient frequency increases (i.e. apparent mass loss) to account for the quantity of HVBr which is being oxidized, and presumably lost to solution as a soluble salt, and the fact that the frequency increases dramatically at the very end of the dissolution process. On the other hand, at lower scan rates the frequency increase is concurrent with the anodic charge consumption, and the slope of the anodic branch indicates loss of one HVBr per electron removed. There are at least two ways to account for slopes which are smaller than expected, one is mixed transport (i.e. simultaneous transport of cations, anions, and/or solvent in such a way as to result in a net mass change of nearly zero), and the other is gross morphological changes of the surface film which lead to solvent trapping in macroscopic pores at the film surface (31) so that the loss of HVBr from the film is offset by the mass of the trapped solvent. A key question which relates to the first possibility is whether the oxidation of HVBr to $HVBr_2$ is initiated at the film/electrode interface and propagates outward towards the solution, or whether the HVBr film has sufficient electronic conductivity for the oxidation to begin at the film/solution interface and propagate inward towards the electrode surface.

The conductivity of these films has not been measured previously, but there are experimental results (6,9c,11a) which indicate that they are, indeed, conductive. For example, the observation of a diffusion controlled CV wave for the reduction of $HVBr_2$ to HVBr, even after the deposition of many equivalent monolayers of HVBr, indicates that HV^{2+} diffusion to the surface rather than charge propagation through the HVBr film is the rate limiting process for the deposition (see Figures 1 and 2 and reference 9c). Given rapid charge propagation across the film, the conversion of HVBr to HV^{2+} should occur at the film/solution interface, and should not require the transport of any ionic species across the HVBr film. These considerations lend support to the second rather than the first of the two possible models described above.

The second (solvent trapping) model suggests the following mechanism for the film dissolution. During the anodic scan the oxidation and dissolution of the HVBr film is initiated by nucleation of pits. These pits grow (laterally and/or downward into the film) in such a way that the HVBr which is being anodically dissolved away is replaced by the supporting electrolyte solution. It has been previously shown that when solution is trapped within the dips and depressions of a imperfectly smooth surface, then the QCM senses this mass as being rigidly attached to the surface (31).For the present case, if the density of this solution is reasonably close to that of the film, then only a small mass change would be expected for replacement of the film by the solution. In the later stages of the dissolution when the nucleated pits have begun to grow together, the film structure will begin to disintegrate, and finally the film will dissolve completely with a relatively abrupt increase in frequency. For this mechanism of film dissolution, one expects the slope of the Δf versus Q plot to steadily increase during the dissolution from a very small value to a very large value in comparison to the slope for the deposition process, in agreement with the experimentally observed trends.

Another possible explanation for these observations is the presence of non-uniform current distribution across the face of the QCM disk electrode. In such a model, the dissolution would be occurring first at the edge of the crystal, where the mass sensitivity is the smallest (39), and then gradually reaching the center of the QCM disk electrode, where the mass sensitivity is the greatest (39). In order to check this possibility, the deposition and dissolution of copper in sulfuric acid was examined with the QCM. These

results, which are reported in a later section, show that such effects are not important for this system under the experimental conditions employed.

If the reduction of HV^{2+} is examined at lower solution concentrations, a prewave is observed ca. 60 mV positive of the bulk diffusion wave. This wave exhibits the characteristics of an adsorption wave in that its peak current depends linearly on the scan rate. The charge under this wave was obtained by manual integration of the area under the curve, which required a rather subjective evaluation of the background. This procedure gave an approximate value of 15 microcoulombs/cm^2 (ca. 1.5×10^{-10} mole/cm^2), which indicates that it arises from reduction of roughly a monolayer of viologen, given a molecular area of 1.0 nm^2 (11). In order to determine whether the wave corresponds to reduction of bulk HV^{2+} to produce adsorbed HV^+ or to reduction of adsorbed HV^{2+} to produce more strongly adsorbed HV^+, we examined the frequency change caused by this redox process. Figure 4 shows the CV and the corresponding QCM data for these conditions. In this figure the QCM data are shown in a derivative representation (see equation 2) so the magnitude of the response may be compared directly to the current. We observe essentially no frequency change coincident with the prewave. Using a molecular area for HVBr of 1.00 nm^2 (11), one calculates that adsorption of a monolayer of HVBr with the molecular plane parallel to the electrode surface should result in a frequency decrease of 4 Hz. Thus, the magnitude of the frequency change we observe at the prewave does not appear to be consistent with the model of adsorption of HV^+ following its reduction from bulk HV^{2+}.

Another possibility is that the HV^{2+} is adsorbed at potentials positive of -0.5 V and that the prewave results from reduction of the adsorbed species. For this case, depending on whether the HV^{2+} is adsorbed with or without coadsorbed anions, one expects a much smaller frequency change upon reduction. For example, if a monolayer of HV^{2+} adsorbs without anion coadsorption, then reduction should lead to a frequency decrease of ca. 1 Hz due to association of bromide anion with the adsorbed HV^+. For the anion coadsorption case, reduction may well lead to no net frequency change if the proper number of anions is adsorbed to form the neutral HVBr deposit. Surface enhanced Raman studies of HV^{2+} at silver electrodes have indicated adsorption of HV^{2+} for potentials negative of -0.2 (20), findings which are analogous with the interpretation of the present results. In addition, several studies of methyl viologen and methyltetradecyl viologen adsorption at gold, silver, platinum,

and mercury electrodes using a variety of electrochemical and spectroscopic techniques reveal adsorption of these species at these concentrations and similarly positive potentials (10a,10b,10d,12,14,22). Thus, we favor an interpretation of the data in which roughly a monolayer of HV^{2+} is adsorbed at the gold electrode surface prior to its reduction to the HVBr state, with reduction and deposition of the solution phase material occurring on top of this adsorbed layer.

When the CV experiments are carried out at higher KBr concentrations one begins to observe the appearance of a new anodic wave on the positive scan at potentials more positive than that of the single wave observed at lower concentrations. This behavior is shown in Figure 5. This wave also appears at lower KBr concentrations if the scan rate is decreased. This wave has been reported by several groups (3b,9a,9c,20), and has been described as resulting from the dissolution of regions of the HVBr deposit which have recrystallized and are therefore more difficult to reoxidize. Figure 5c shows the Δf versus Q plot for this scan. The salient feature of the plot is that the slope of the anodic branch is the same for both anodic waves. This implies that after the recrystallization the stripping of the film still occurs with removal of one HVBr formula unit per electron extracted from the film, and that the composition of the recrystallized film is probably quite similar to that of the initial deposit. A further conclusion based on these data is that the QCM appears to be relatively insensitive to the physical state of the deposit on the electrode surface. This has been previously reported for the case of QCM studies of ion and solvent transport in thin films of poly(aniline) on electrodes (26b). An implication of this behavior is that the QCM response does not depend strongly on the materials properties of the deposit, as expected for a layer which is behaving elastically.

Potential Step Methods. A potential problem in application of the QCM to studies of thin film deposition is whether or not the film displays elastic behavior. Use of the Sauerbrey equation assumes that the film is elastic, and therefore does not experience shear during the measurement. To the extent that the film does experience shear, then some degree of mass sensitivity will be lost and the frequency changes which are observed will not be a true measure of the mass change at the surface. This has been recognized for some time and various approaches to remedy the problem have been presented, including both theoretical and empirical calibration methods (26,27d,37b). A manifestation of

non-elastic behavior is the loss of mass sensitivity as the film thickness increases due to damping of the shear wave within the film. Thus, if it can be shown that the mass sensitivity remains constant for a range of film thicknesses, then elastic behavior is definitively demonstrated. Potential step methods were chosen for this purpose.

When the electrode potential is stepped well past the reduction potential of HV^{2+}, but not into the region of reduction to the neutral HV species, the deposition of HVBr begins almost immediately. The time course of the deposition has been shown to follow nucleation kinetics at relatively short times with semi-infinite diffusion controlling the current at longer times (3a,9a,11). For potential steps well over the wave, the integrated Cottrell equation gives the total amount of material which has reached the surface at a given time. In the present case of deposition of the reduced HV^{+} in the form of HVBr with 100% efficiency, this equation should give the total mass deposited during the potential step, given the molar mass of the depositing species, its concentration, and diffusion coefficient. Equation 4 gives the dependence of the frequency change (Δf, in Hz) on the time (t, in seconds) after the step:

$$\Delta f = (2 \times 10^6)\ K\ MW_f\ D^{1/2}\ C\ t^{1/2}\ \pi^{-1/2} \qquad (4)$$

where D is the diffusion coefficient (in cm^2/s), C is the concentration of the diffusing species (in $mole/cm^3$), K is the proportionality constant described above (in $Hz/microgram/cm^2$), and MW_f is the apparent molar mass of the depositing species which forms the film (in grams/mole). Note that in the present case MW_f may be larger than the molar mass of HVBr if solvent and/or ionic species were to be incorporated into the film during its formation. The slope of a plot of Δf versus $t^{1/2}$ may be used to calculate MW_f, given D and C.

A more direct measure of MW_f may be obtained by using the slopes of the Δf versus $t^{1/2}$ and the Q versus $t^{1/2}$ plots. We denote these slopes as S_f (in $Hz/s^{1/2}$) and S_q (in $(Coul/cm^2)/s^{1/2}$), respectively. Equation 5 gives the value of MW_f calculated from the ratio of these slopes:

$$(S_f / S_q) * (10^6\ F / K) = MW_f \qquad (5)$$

with all of the variables having been previously described. This method of arriving at a value of MW_f does not require knowledge of either the diffusion coefficient or the concentration, since both slopes depend on these quantities in the same way.

Figure 6a shows the result of a typical potential step experiment. The QCM frequency drops continuously after the potential step, indicating mass gain at the surface due to HVBr deposition. Figure 6b shows the plot of Δf versus $t^{1/2}$ (the microgravimetric equivalent of an Anson plot) for this experiment. The linearity of the plot indicates the general applicability of Equation 4. Table 2 gives the MW_f values evaluated from equation 5 for several step experiments of this type at two different $HVBr_2$ concentrations and with several final potentials. These MW_f values are seen to be strongly dependent on the value of the final potential. When the final potential is well past the wave, the value of MW_f is essentially equal to the molar mass of HVBr. For steps to less negative potentials the value increases dramatically, especially at the foot of the wave. We propose that this behavior is related to the number of nucleation sites created during the potential step. For steps to very negative potentials, a large number density of nucleation sites is produced at the surface, and the growth of the film is essentially uniform. For steps to less negative potentials, a smaller number density of nucleation sites is created. These nuclei grow hemispherically, and the surface roughness of the newly formed HVBr film increases. This causes trapping of solution within the pores, as described above, and leads to anomalously large calculated values of MW_f. The agreement of the value obtained for MW_f with the molar mass of HVBr for very negative potential steps is strong evidence that the film deposits as the HVBr salt, with essentially no incorporation of either solvent or ionic species from the supporting electrolyte.

The observation of linearity for these microgravimetric Anson plots for times and frequency changes much larger than those observed in the potential sweep experiments implies that these HVBr films exhibit elastic behavior for all thicknesses used in the present study. If the films were not exhibiting elastic behavior, then the plots would have concave (downward) curvature due to an increasing loss of mass sensitivity as the film thickness increased. Again, it is significant that the recrystallization which occurs in these films at times longer than a few seconds for HV^{2+} concentrations larger than a few millimolar does not appear to affect the QCM frequency response. We have not searched for the breakdown of elastic behavior which is expected at much larger thicknesses.

Double potential step experiments were done in an effort to observe the dissolution of the HVBr films during the oxidative step. The anodic charge is

passed in a very short time, indicating that film dissolution must be quite fast. The frequency also indicates that the film is lost from the surface very rapidly after the positive step. In fact, the film is lost from the surface so quickly that the QCM is unable to elucidate the temporal details of the dissolution. This is probably due to intrinsic limitations of the QCM for response to fast processes. This point will be further addressed in a future communication.

Copper Deposition. As mentioned above, a problem which could be encountered in studies of this type is the possible presence of non-uniform current density distribution across the face of the QCM disk electrode. Past studies have shown that the mass sensitivity varies across the face of the QCM electrode, with the dependence of this radial mass sensitivity depending on the details of the electrode size, electrode placement, and the crystal preparation. For example, for crystals having both faces exactly planar the mass sensitive region extends slightly past the outer radius of the electrode, while for plano-convex crystals the mass sensitive region is nearly completely confined within the radius of the electrode (40). In both cases, the mass sensitivity varies in a Gaussian manner with the radial distance from the center of the crystal (39,40). The mass sensitivity expressed in the Sauerbrey equation is based on an assumption that the film is deposited uniformly across the face of the crystal electrodes, so that the integral mass sensitivity remains constant for any film thickness (so long as the loading is not too great).

Many previous studies of the current distribution at disk electrodes have shown that under different conditions the current density distribution may be either uniform or non-uniform. In particular, both Bruckenstein and Miller (41) and Marathe and Newman (42) have studied the influence of these effects for the case of copper deposition from acidic sulfate solutions. Both studies showed that uniform current density distribution tends to occur at low concentrations of the redox species and high supporting electrolyte concentrations, and vice versa. Thus, the former conditions are required in order to make meaningful, quantitative measurements of mass changes during QCM/electrochemical experiments.

To show unequivocally that the HV^{2+} experiments reported here are not influenced by non-uniform current density distributions, the deposition of copper on the QCM was studied with both potential step and potential sweep

methods using exactly the same conditions as those in the $HV2^+$ experiments, i.e. identical ionic strength and concentration of the redox species. Figure 7a shows a representative example of a plot of Δf versus Q observed for a sweep experiment. The salient feature of the plot is the linearity for both the reductive and oxidative branches, indicative of a constant mass sensitivity both at the foot of the wave (where the current density is expected to be the least uniform) and past the peak, where the reduction process is diffusion controlled. Thus, the hysterisis observed for the $HV2^+$ reoxidation is not caused by non-uniform current density distribution. Figure 7b shows a typical gravimetric Anson plot for a potential step experiment under the same conditions, and demonstrates the extremely good linearity of these plots.

CONCLUSIONS

This study of the mass changes which occur at the electrode during HVBr deposition and dissolution has revealed several interesting aspects in its electrochemical behavior. Based on the excellent agreement between the microgravimetric Anson plot slopes and the formula mass of HVBr, it can be inferred that little, if any, supporting electrolyte is incorporated into the HVBr film for potential step deposition at potentials well past the first reduction wave. On the other hand, for deposition by potential sweep the values of MW_f given in Table 1 indicate that, under certain conditions, the film is deposited with a rough surface with a consequent trapping of solution within these pores.

Under the conditions used in this work (i.e. low concentration of $HV2^+$ and high ionic strength) the film is deposited fairly uniformly across the face of the QCM disk electrode, as expected based on the early analyses of current distribution at a disk electrode (41,42) and as indicated by the present results for copper deposition. Another conclusion based on the excellent agreement of the microgravimetric Anson plot slopes and the formula mass of HVBr is that the film deposits with a relatively low surface roughness, because the known influence of surface roughness (31) is to increase the apparent mass by including trapped supporting electrolyte in the mass measured by the resonator. Thus, the model which develops is one of deposition to form a reasonably uniform, compact film with a current efficiency for deposition of essentially 100%.

The presence of a cathodic adsorption prewave positive of the bulk diffusion wave was observed in the voltammetry of HV^{2+} on the QCM gold electrodes. Correlation of the cathodic charge with the very small mass changes concurrent with this wave indicates that it arises from reduction of adsorbed HV^{2+} to even more strongly adsorbed HV^{+}, rather than from reduction of solution phase dication followed by adsorption. Lu and Cotton (20) have investigated the adsorption of HV^{2+} onto silver electrodes by surface enhanced Raman spectroscopy. They find evidence for strong adsorption of HV^{2+} for potentials negative of -0.2 V following oxidation-reduction cycling of the electrode in the presence of HV^{2+} in solution. Based on the dependence of the SER spectra on the concentration of bromide in the solution, they postulate that in the absence of bromide, HV^{2+} adsorbs directly onto the electrode surface, while in the presence of bromide at concentrations above ca. 10^{-4}, HV^{2+} adsorbs onto the electrode via an ion pair interaction with adsorbed bromide ion. In the present case, since (in the absence of HV^{2+}) bromide does not appear to be adsorbed on gold at potentials negative of 0.0 V (43), we suspect that HV^{2+} adsorbs directly onto the gold electrode. While coadsorption of bromide onto the surface may be induced by the presence of HV^{2+}, the signal to noise ratio of the frequency measurements is not sufficient to distinguish whether the HV^{2+} adsorbs with or without coadsorbed bromide.

The finding that the film dissolution seems to be initiated at the film/solution interface by pit nucleation lends credence to Jasinski's early assertion (6) that the film is an electronic conductor. Thus, during the anodic dissolution, charge propagates across the film rapidly, with little dissolution occurring until the holes reach the film/solution interface. Also, based on the scan rate dependence of the hysterisis in the frequency versus charge plots, one can speculate on whether the pit nucleation is instantaneous or progressive. We favor progressive nucleation based on the following reasoning. At high scan rates, the number of nuclei is relatively small, so that large pits are created as the pits grow down and/or laterally in the film. When these large pits finally merge and the film disintegrates, the frequency increases dramatically. At low scan rates, the number of nuclei is much larger due to the longer time in which they are allowed to form. In the limit of an infinitely slow scan, the areal density of nucleation sites gets arbitrarily large, and the film dissolution becomes perfectly uniform. Thus, at lower scan rates the film dissolves uniformly, and one expects no

hysterisis in the frequency versus charge plots. While this explanation is clearly speculative, this type of problem should lend itself to more detailed solution by simulation methods. We are currently developing such methods to address these and other questions related to mass changes which are consequent to redox processes involving adsorbed species.

The use of potential step methods to determine the apparent mass of a depositing species from the slope of the microgravimetric Anson plot represents a useful new tool for characterizing the electrodeposition of thin films on electrode surfaces. In certain cases a great deal of information may be obtained from such studies. For example, in the present study the excellent agreement of the microgravimetric Anson plot slopes with the expected values strongly indicates that the deposition gives a fairly uniform, compact film. Also, a very high current efficiency can be inferred from these data. For cases in which the slopes do not agree with the value expected based on simple deposition to give a uniform, compact film, the discrepancy could have its origin in any of several effects, which in some cases may be distinguishable by examining the time dependence of the discrepancy. These include but are not limited to control of the rate of deposition by some process other than diffusion (such as nucleation), non-uniform deposition, less than 100% current efficiency for the deposition, a stoichiometry for the film which is different than that anticipated, and incorporation of solvent and/or supporting electrolyte into the film.

In closely examining the frequency change as a function of time at very short times after potential steps, we have observed that a limit on the temporal resolution of the QCM exists. Plots of frequency versus time always show intercepts on the positive time axis, and these appear to be very similar for many different types of systems (e.g. HVBr deposition and ion and/or solvent incorporation into poly(vinylferrocene) (44) and poly(nitrostyrene) (45) films following potential steps over their oxidation and reduction waves, respectively). We are examining this effect in more detail, but suspect that it is related to the Q value of the crystal (i.e. the ratio of stored to dissipated energy per cycle for the resonator). Thus, for situations in which the Q value is large (e.g. in vacuum or gas phase work) the mass measurements may be made relatively rapidly, while for low Q applications (e.g. in solutions) the measurements will probably require longer times.

ACKNOWLEDGEMENTS

We gratefully acknowledge support of this work by the Office of Naval Research and the National Science Foundation (RII-8610680). We also thank Dr. Owen Melroy for several enlightening discussions and for communicating to us some early results in this area.

REFERENCES

(1a) C. J. Schoot, J. J. Ponjee, H. T. Van Dam, R. A. Van Doorn and P. T. Bolwijn, Appl. Phys. Lett., 23, No. 2 (1973) 64.

(1b) H. T. van Dam and J. J. Ponjee, J. Electrochem. Soc., 121, No. 12 (1974) 1555.

(2a) I. F. Chang, B. L. Gilbert and T. I. Sun, J. Electrochem. Soc., 122, No. 7 (1980) 955.

(2b) I. F. Chang and W. E. Howard, IEEE Trans. Elec. Dev., 22, No. 9 (1975) 749.

(3a) J. Bruinink and C. G. A. Kregting, J. Electrochem. Soc., 125, No. 9 (1978) 1397.

(3b) J. Bruinink, C. G. A. Kregting and J. J. Ponjee, J. Electrochem. Soc., 124, No. 12 (1977) 1854.

(3c) J. Bruinink and P. Van Zanten, J. Electrochem. Soc., 124, No. 8 (1977) 1232.

(4a) G. G. Barna and J. G. Fish, J. Electrochem. Soc., 128, No. 6 (1981) 1290.

(4b) G. G. Barna, J Electrochem. Soc., 127, No. 6 (1980) 1317.

(5) J. M. Calvert, T. J. Manuccia and R. J. Nowak, J. Electrochem. Soc., 133, No. 5 (1986) 951.

(6a) R. J. Jasinski, J. Electrochem. Soc., 124, No. 5 (1977) 637.

(6b) R. J. Jasinski, J. Electrochem. Soc., 125, No. 10, (1978) 1619.

(6c) R. Jasinski, J. Electrochem. Soc., 126, No. 1 (1979) 167.

(7) K. Belinko, Appl. Phys. Lett., 29, No. 6 (1976) 363.

(8) A. F. Sammells and N. U. Pujare, J. Electrochem. Soc., 133,

No. 6 (1986) 1270.

(9a) A. Bewick, A. C. Lowe and C. W. Wederell, Electrochim. Acta, 28, No. 12, (1983) 1899.

(9b) D. J. Barclay, B. F. Dowden, A. C. Lowe and J. C. Wood, Appl. Phys. Lett., 42, No. 10 (1983) 911.

(9c) A. Bewick, D. W. Cunningham and A. C. Lowe, Makromol. Chem., Macromol. Symp., 8 (1987) 355.

(10a) O. Enea, Electrochim. Acta, 31, No. 7 (1986) 789.

(10b) B. Beden, O. Enea, F. Hahn and C. Lamy, J. Electroanal. Chem., 170, (1984) 357.

(10c) P. Crouigneau, O. Enea and C. Lamy, Nouv. J. Chim., 10 No. 10 (1986) 539.

(10d) P. Crouigneau, O. Enea and B. Beden, J. Electroanal. Chem., 218 (1987) 307.

(11a) B. Scharifker and C. Wehrmann, J. Electroanal. Chem., 185 (1985) 93.

(11b) S. Fletcher, L. Duff and R. G. Barradas, J. Electroanal. Chem., 100 (1979) 759.

(12) M. Heyrovsky and L. Novotny, Coll. Czech. Chem. Commun., 52 (1987) 1097.

(13) A. Yasuda, H. Kondo, M. Itabashi and J. Seto, J. Electroanal. Chem., 210 (1986) 265.

(14) K. Kobayashi, F. Fujisaki, T. Yoshimine and K. Niki, Bull. Chem. Soc. Jpn., 59, (1986) 3715.

(15) N. J. Goddard, A. C. Jackson and M. G. Thomas, J. Electroanal. Chem., 159 (1983) 325.

(16) D. C. Bookbinder and M. S. Wrighton, J. Electrochem. Soc.,

130, No. 5 (1983) 1080.

(17) A. Yasuda, H. Mori, Y. Takehana, A. Ohkoshi and N. Kamiya, J. Appl. Electrochem. 14 (1984) 323.

(18) J. A. Barltrop and A. C. Jackson, J. Chem. Soc. Perkin Trans. II (1984) 367.

(19) A. Goldon and J. Przyluski, Electrochim. Acta, 30, No.9 (1985) 1231.

(20) T. Lu and T. M. Cotton, J. Phys. Chem., 91, (1987) 5978.

(21) C. A. Melendres, P. C. Lee and D. Meisel, J. Electrochem. Soc., 130, No. 7 (1983) 1523.

(22) A. Regis and J. Corset, J. Chim. Phys., 78, No. 9 (1981) 687.

(23) M. Datta, R. E. Jansson and J. J. Freeman, Appl. Spect., 40, No. 2 (1986) 251.

(24a) T. Sawada and A. J. Bard, J. of Photoacoustics, 1, No. 3 (1982-83) 317.

(24b) B. Reichman, F. F. Fan and A. J. Bard, J. Electrochem. Soc., 127 No. 2 (1980) 333.

(24c) R. E. Melpas and A. J. Bard, Anal. Chem., 52 (1980) 109.

(24d) G. H. Brilmyer and A. J. Bard, Anal. Chem., 52 (1980) 685.

(25a) R. Cieslinski and N. R. Armstrong, J. Electroanal. Chem., 161, (1984) 59.

(25b) R. Cieslinski and N. R. Armstrong, J. Electrochem. Soc., 127, No. 12 (1980) 2605.

(26a) P. T. Varineau and D. A. Buttry, J. Phys. Chem., 91 (1987) 1292.

(26b) D. Orata and D. A. Buttry, J. Am. Chem. Soc., 109 (1987) 3574.

(26c) J. Donohue, L. Nordyke and D. A. Buttry, Proceedings of the

Second Chemically Modified Surfaces Symposium, D. Leyden and W. Collins, eds.; Gordon and Breach, N.Y., in press.

(27a) J. H. Kaufman, K. K. Kanazawa and G. B. Street., Phys. Rev. Lett., 53 (1984) 2461.

(27b) O. Melroy, K. Kanazawa, J. G. Gordon II and D. A. Buttry, Langmuir, 2, No. 6 (1986) 697.

(27c) M. R. Deakin and O. Melroy, J. Electroanal. Chem., 239 (1988) 321.

(27d) E. Grabbe, R. P. Buck and O. Melroy, J. Electroanal Chem., 223 (1987) 67.

(28a) S. Bruckenstein and M. Shay, J. Electroanal. Chem., 188 (1985) 131.

(28b) S. Bruckenstein and S. Swathirajar, Electrochim Acta, 30 (1985) 851.

(28c) S. Bruckenstein and M. Shay, Electrochim. Acta, 30 (1985) 1295.

(29a) W. Stoeckel and R. Schumacher, Ber. Bunsen - Ges. Phys. Chem., 91 (1987) 345.

(29b) R. Schumacher, A. Mueller and W. Stoeckel, J. Electroanal. Chem., 219 (1987) 311.

(30) M. Benje, M. Eiermann, U. Pittermann and Komrad Weil, Ber. Bunsen - Ges. Phys. Chem., 90 (1986) 435.

(31a) R. Schumacher, G. Borges and K. K. Kanazawa, Surf. Sci., 163 (1985) L621.

(31b) R. Schumacher, J. G. Gordon and O. Melroy, J. Electroanal. Chem., 216 (1987) 127.

(32) see, for example, R. W. Murray, in "Electroanalytical

Chemistry", A. J. Bard, ed., Vol. 13, Marcel Dekker, N.Y., 1984.

(33) K. Hoshino and T. Saji, J. Am. Chem. Soc., 109 (1987) 5881.

(34) G. Sauerbrey, Z. Physik., 155 (1959) 206.

(35) C. Lu and O. Lewis, J. Appl. Phys., 43 (1972) 4385.

(36) E. Benes, J. Appl. Phys., 56 (1984) 608.

(37a) K. K. Kanazawa and J G. Gordon, Anal. Chem., 57 (1985) 1770.

(37b) K. K. Kanazawa preprint

(38a) T. Berzins and P. Delahay, J. Am. Chem. Soc., 75 (1953) 555.

(38b) M. M. Nicholson, J. Am. Chem. Soc., 79 (1957) 7.

(39a) S. Fletcher, J. Electroanal. Chem., 118 (1981) 419.

(39b) M. D. Pritzker, J. Electroanal. Chem., 243 (1988) 57.

(40) D. M. Ullevig, J. F. Evans and M. G. Albrecht, Anal. Chem., 54 (1982) 2341.

(41) H. K. Pulker, E. Benes, D. Hammer and E. Sollner, Thin Solid Films, 32 (1976) 27.

(42) S. Bruckenstein and B. Miller, J. Electrochem. Soc., 117, No. 8 (1970) 1044.

(43) V. Marathe and J. Newman, J Electrochem. Soc., 116, No. 12, (1969) 1704.

TABLE 1

Concentration of $HVBr_2$ (mM)	Scan Rate (mV/s)	Concentration of KBr (M)	MW_f (g/mole)
1	10	0.3	496
1	25	0.3	512
1	50	0.3	535
1	100	0.3	511
1	200	0.3	571
1	25	3.0	443
1	50	3.0	528
1	100	3.0	736
1	200	3.0	654
5	10	0.3	411
5	25	0.3	474
5	50	0.3	410
5	100	0.3	424
5	200	0.3	472
5	10	3.0	623
5	25	3.0	680
5	50	3.0	678
5	100	3.0	652
5	200	3.0	729

TABLE 2

Concentration of $HVBr_2$ (mM)	Concentration of KBr (M)	Final Potential (V)	MW_f (g/mole)
1	0.3	-0.580	866
1	0.3	-0.600	731
1	0.3	-0.750	449
5	0.3	-0.535	1205
5	0.3	-0.536	1145
5	0.3	-0.537	957
5	0.3	-0.538	926
5	0.3	-0.750	460

FIGURE CAPTIONS

1. CV/QCM steady state scan from 0.0 to -1.1 V in 1.0 mM $HVBr_2$, 0.3 M KBr, and 5 mM NaOH. Scan rate 100 mV/s. a) CV response. b) QCM frequency response.

2. CV/QCM steady state scan from 0.2 to -0.65 V of 5 mM viologen, 0.3 M KBr, and 5 mM NaOH. Scan Rate 50 mV/s. a) CV response. b) QCM frequency response.

3. Plot of Δf versus Q for CV from 0.2 to -0.65 V. All conditions as in Figure 2 except scan rate. a) 50 mV/s. b) 100 mV/s. c) 200 mV/s.

4. a) Plot of the CV scan from +0.2 to -0.65 V of 0.2 mM viologen, 0.3 M KBr, and 5 mM NaOH. Scan rate 10 mV/s (solid line). b) Plot of the derivative of the frequency response versus the potential for the same scan as in Figure 4a (dashed line).

5. CV/QCM steady state scan from +0.2 to -0.65 V of 5 mM viologen, 2.0 M KBr, and 5 mM NaOH. Scan Rate 10 mV/s. a) CV response. b) QCM frequency response. c) Plot of Δf versus Q.

6. a) Relative frequency change versus time for 10 sec step from +0.2 to -0.57 V for a solution containing 5 mM $HVBr_2$, 0.3 M KBr, and 5 mM NaOH. b) Plot of the relative frequency change versus the square root of time for the same step as in Figure 6a.

7. a) Plot of Δf versus Q for a CV scan from 0.6 to -0.2 V for 5 mM $CuSO_4$ in 0.3 M H_2SO_4. Scan rate 50 mV/s. b) Plot of Δf versus $t^{1/2}$ reductive step from 0.35 to -.25 V for 5 mM $CuSO_4$ SO_4 in 0.3 M H_2SO_4.

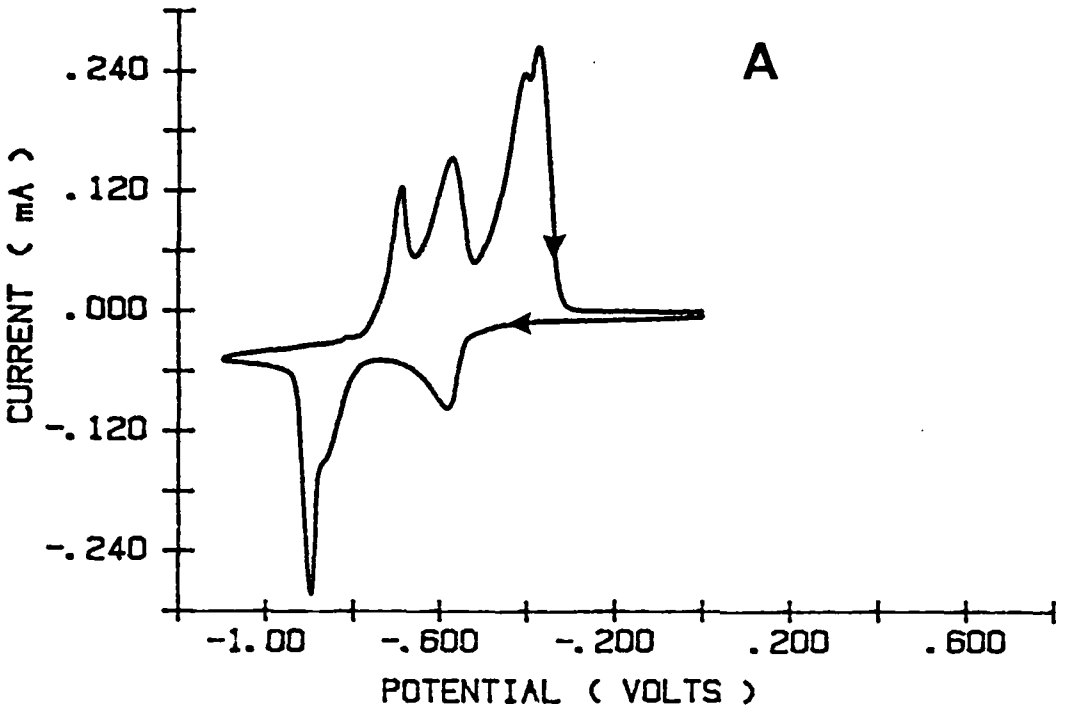
A
.240
.120
.000
-.120
-.240
CURRENT (mA)
-1.00
-.600
-.200
.200
.600
POTENTIAL (VOLTS)

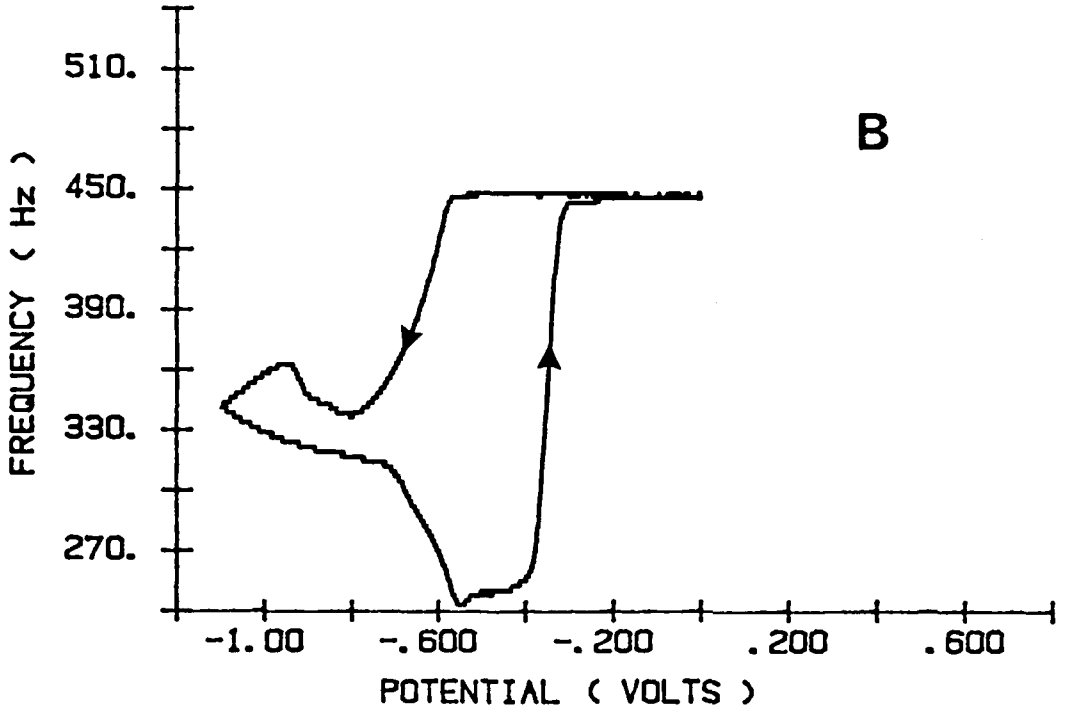
B
510.
450.
390.
330.
270.
FREQUENCY (Hz)
-1.00
-.600
-.200
.200
.600
POTENTIAL (VOLTS)

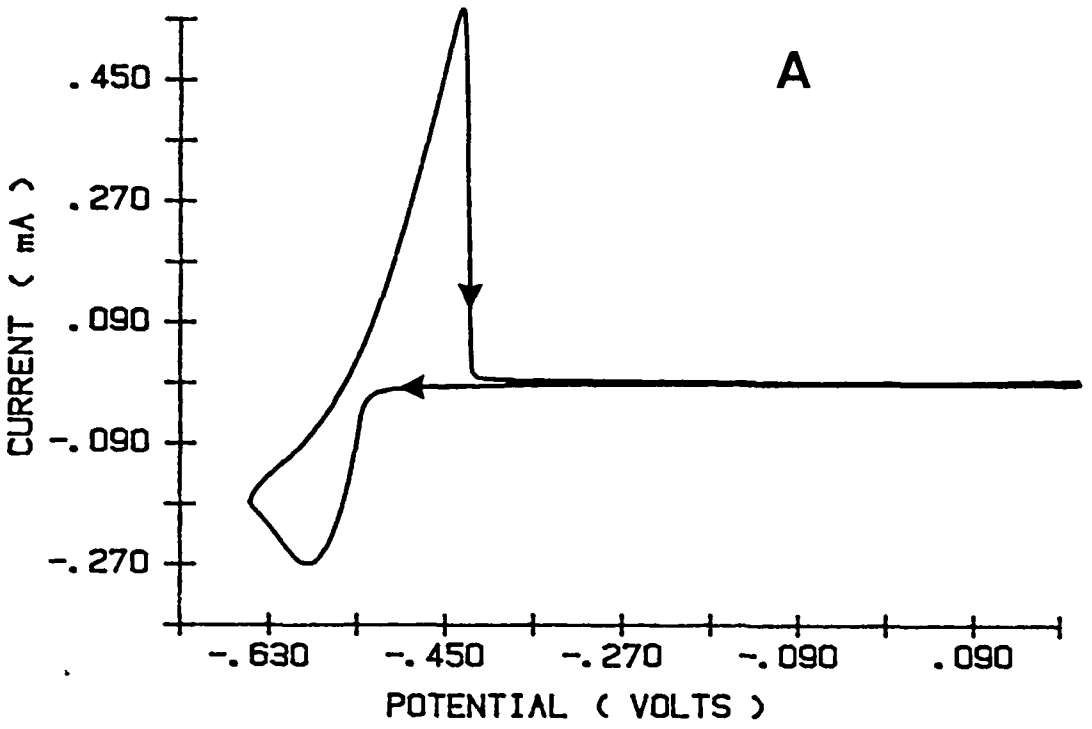
A
.450
.270
.090
-.090
-.270
CURRENT (mA)
-.630
-.450
-.270
-.090
.090
POTENTIAL (VOLTS)

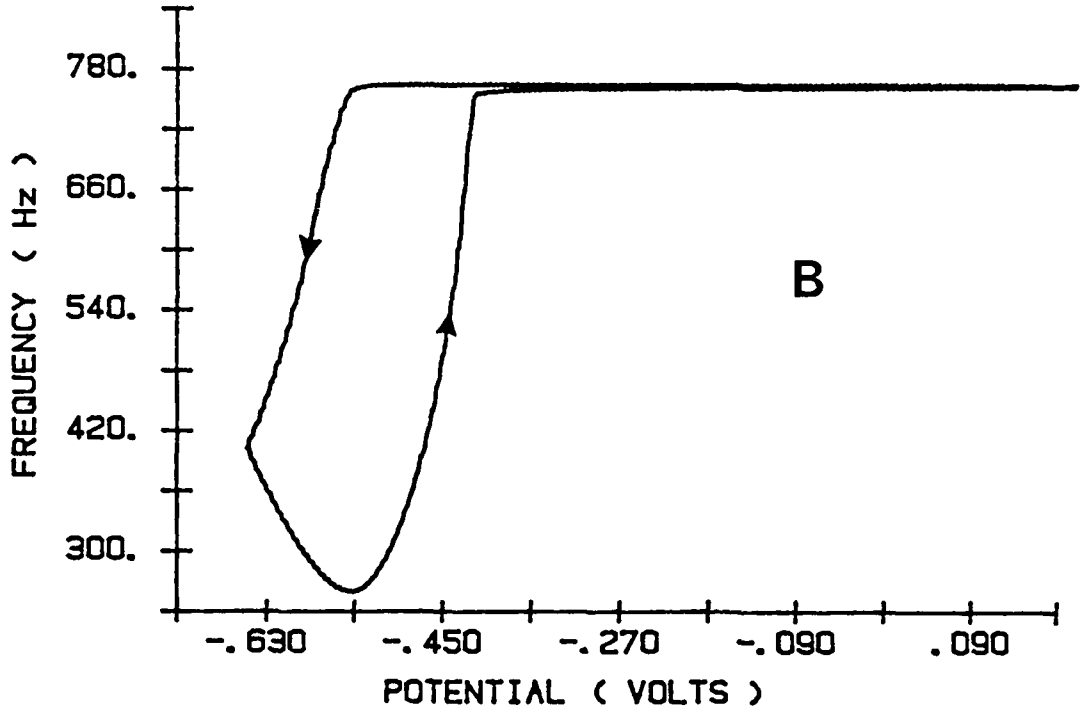
B
780.
660.
540.
420.
300.
FREQUENCY (Hz)
-.630
-.450
-.270
-.090
.090
POTENTIAL (VOLTS)

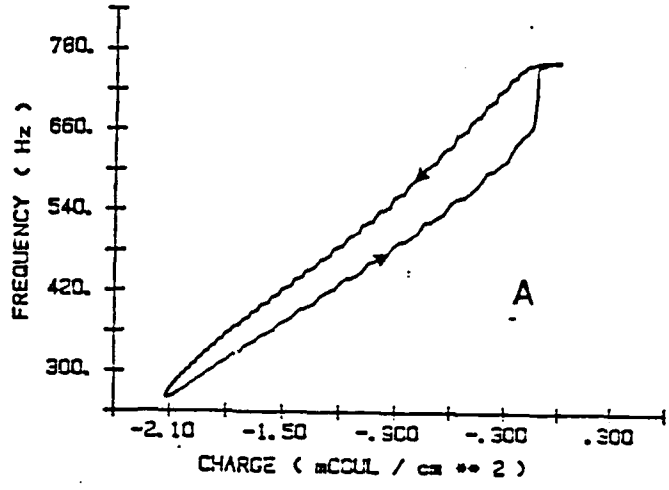
780.
660.
540.
420.
300.
FREQUENCY (Hz)
A
-2.10
-1.50
-.900
-.300
.300
CHARGE (mCOUL / cm ** 2)

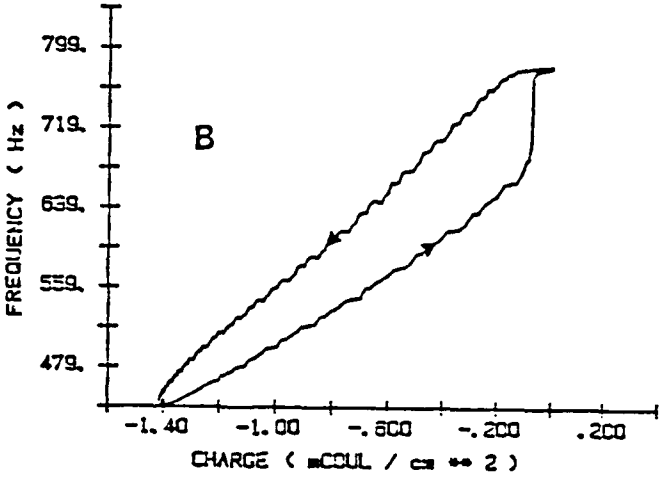
799.
719.
639.
559.
479.
FREQUENCY (Hz)
B
-1.40
-1.00
-.600
-.200
.200
CHARGE (mCOUL / cm ** 2)

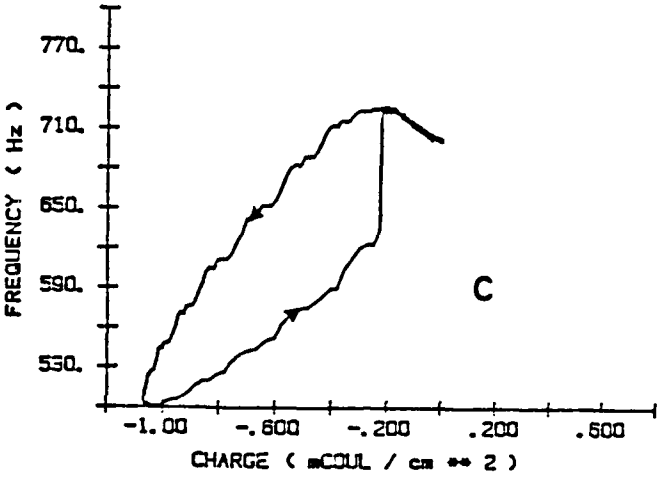
770.
710.
650.
590.
530.
FREQUENCY (Hz)
C
-1.00
-.600
-.200
.200
.600
CHARGE (mCOUL / cm ** 2)

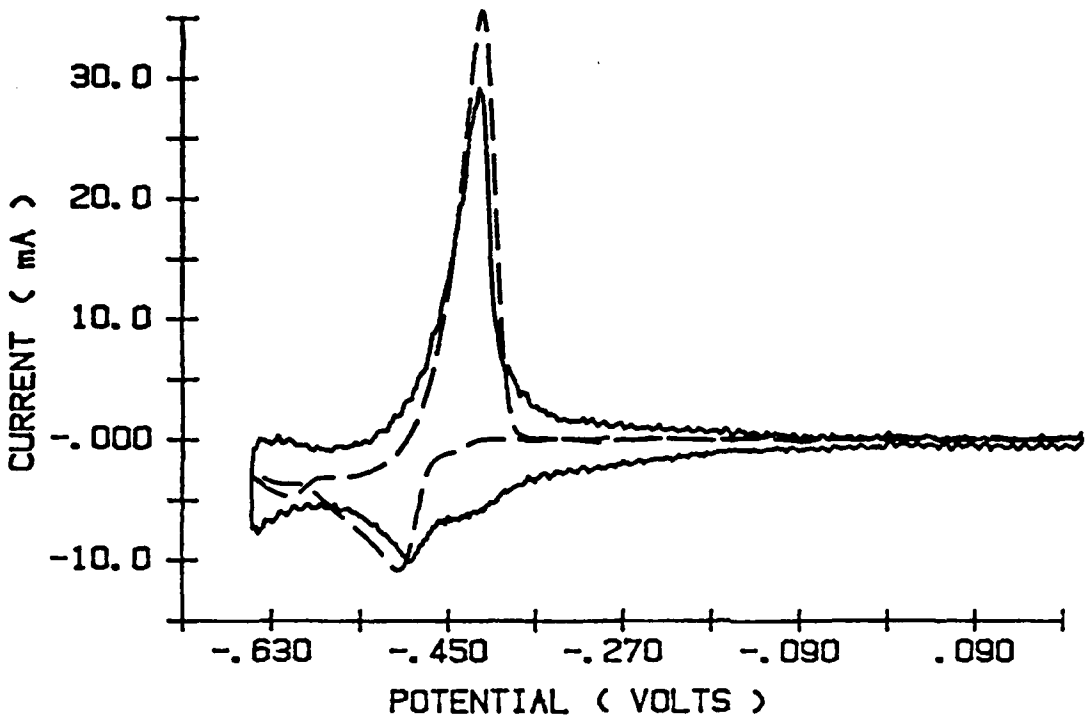
30.0
20.0
10.0
-.000
-10.0
CURRENT (mA)
-.630
-.450
-.270
-.090
.090
POTENTIAL (VOLTS)

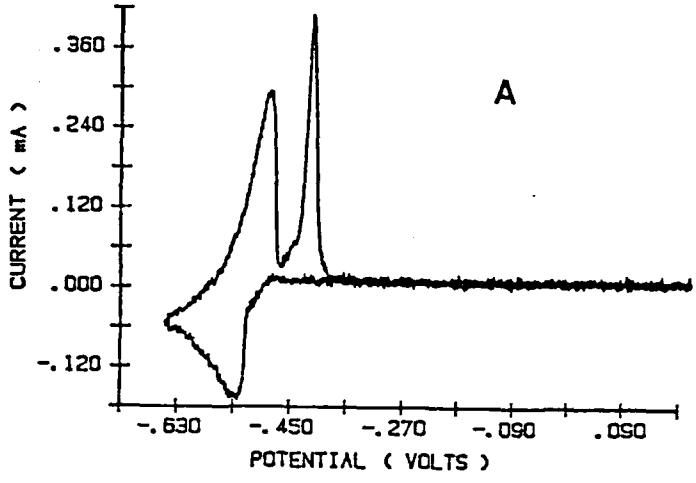
A
.360
.240
.120
.000
-.120
CURRENT (mA)
-.630
-.450
-.270
-.090
.090
POTENTIAL (VOLTS)

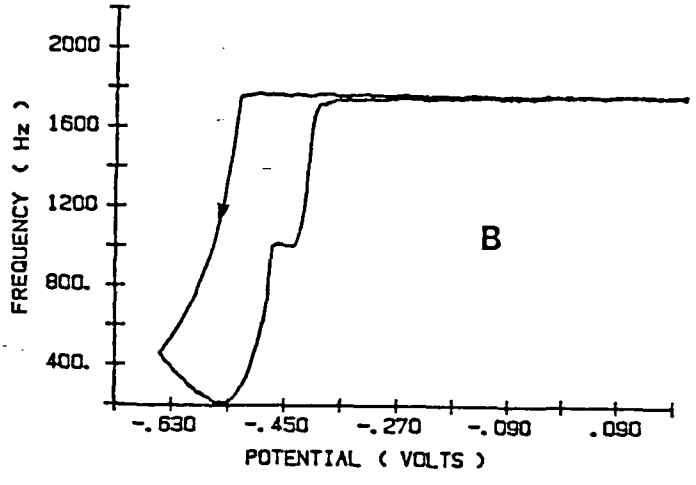
B
2000
1600
1200
800.
400.
FREQUENCY (Hz)
-.630
-.450
-.270
-.090
.090
POTENTIAL (VOLTS)

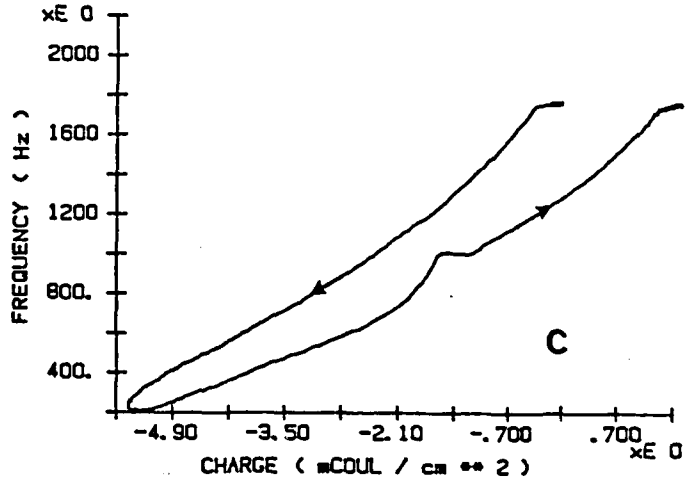
C
xE 0
2000
1600
1200
800.
400.
FREQUENCY (Hz)
-4.90
-3.50
-2.10
-.700
.700
xE 0
CHARGE (mCOUL / cm ** 2)

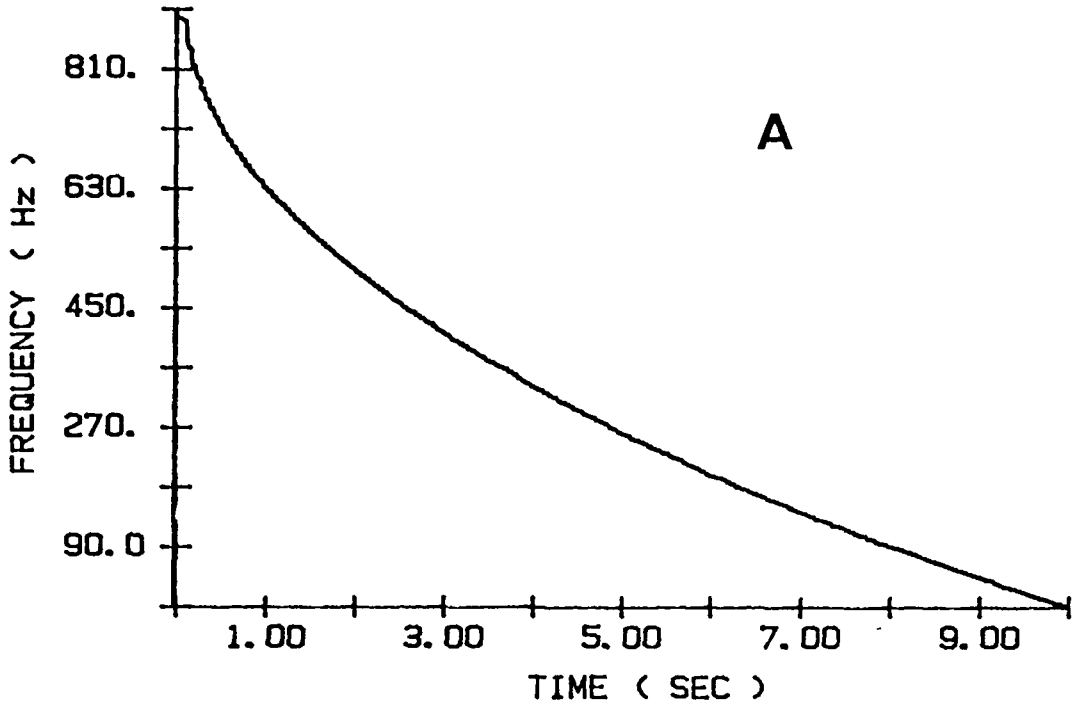
A
810.
630.
450.
270.
90.0
FREQUENCY (Hz)
1.00
3.00
5.00
7.00
9.00
TIME (SEC)

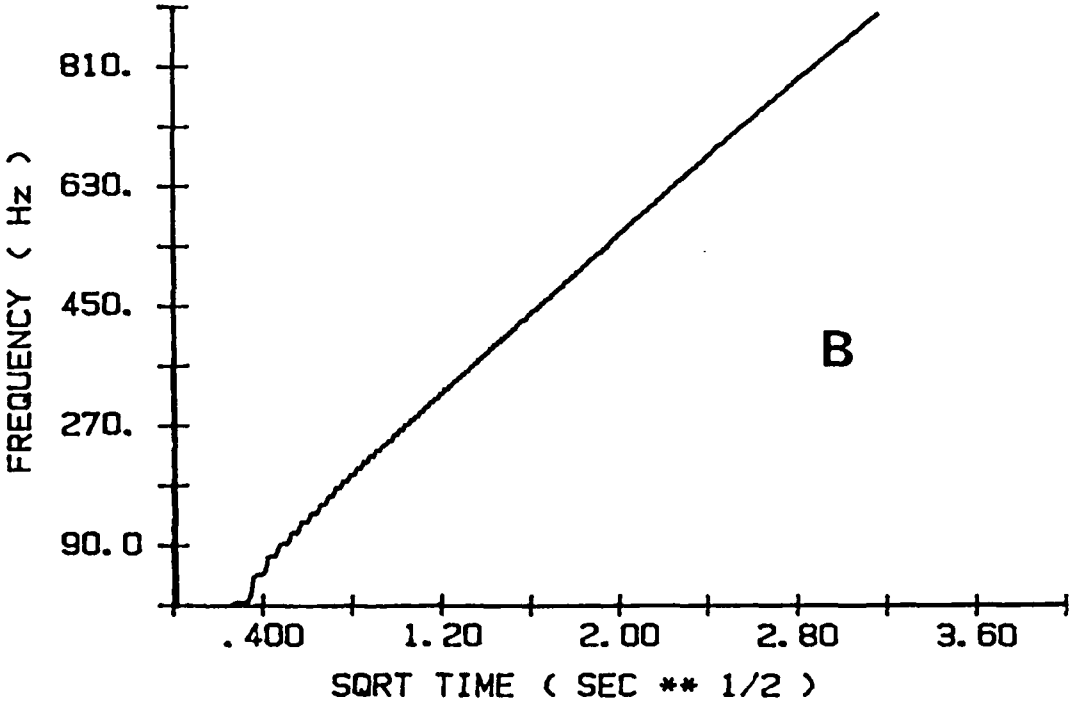
B
810.
630.
450.
270.
90.0
FREQUENCY (Hz)
.400
1.20
2.00
2.80
3.60
SQRT TIME (SEC ** 1/2)

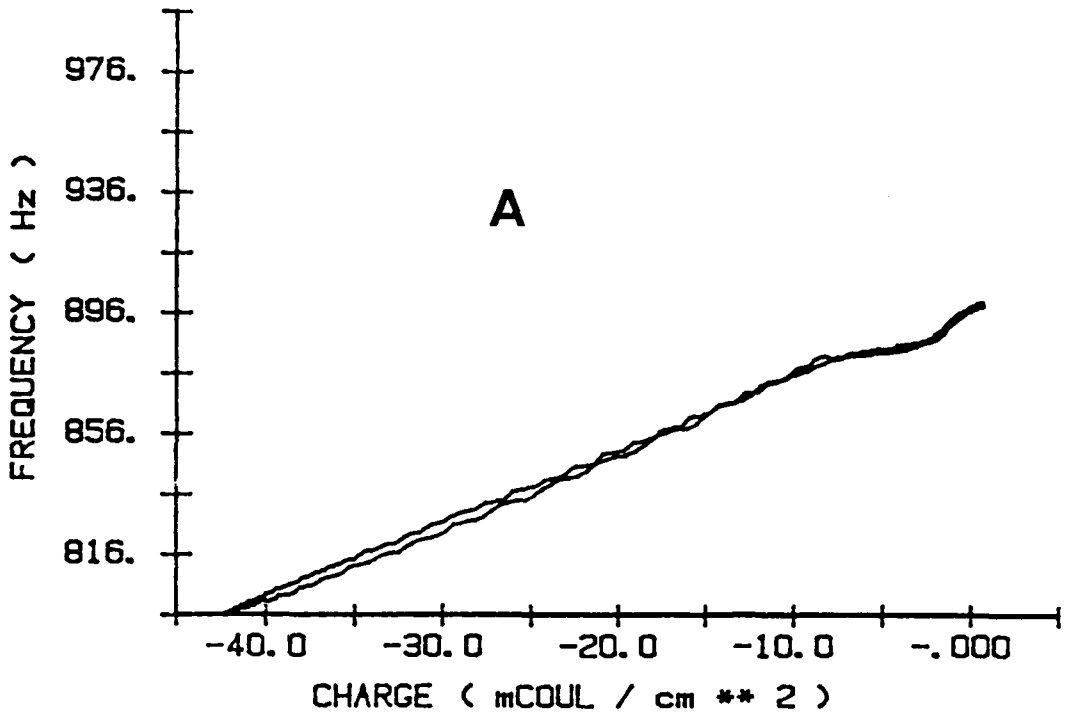
976.
936.
896.
856.
816.
FREQUENCY (Hz)
A
-40.0
-30.0
-20.0
-10.0
-.000
CHARGE (mCOUL / cm ** 2)

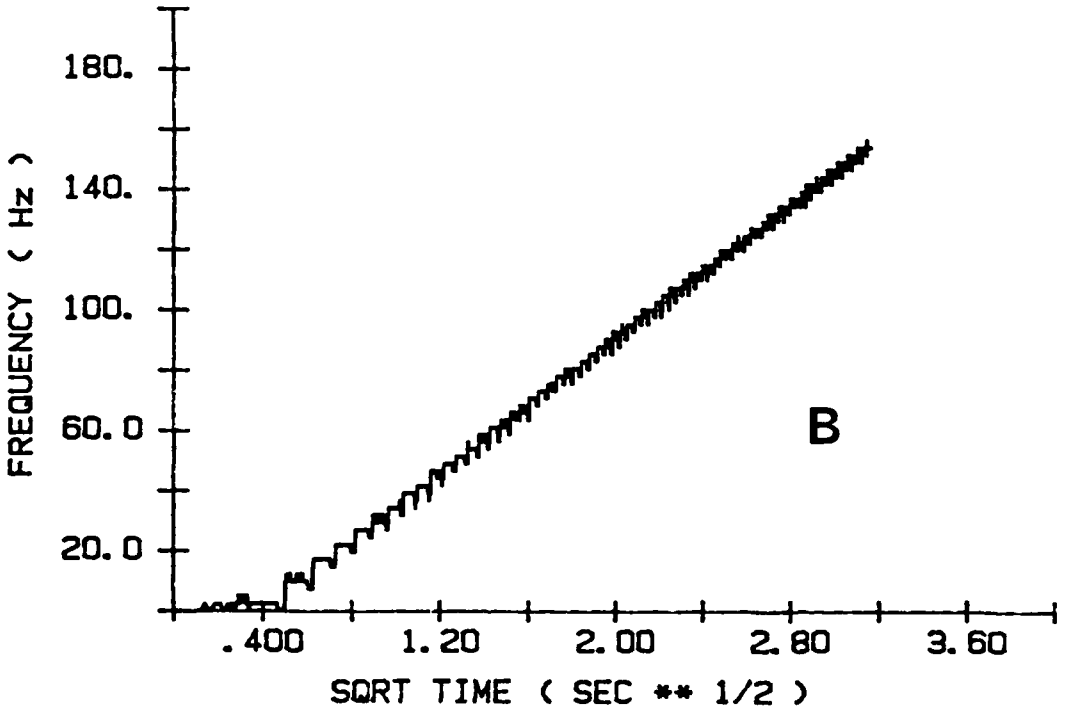
180.
140.
100.
60.0
20.0
FREQUENCY (Hz)
B
.400
1.20
2.00
2.80
3.60
SQRT TIME (SEC ** 1/2)

TECHNICAL REPORT DISTRIBUTION LIST, GEN

	No. Copies
Office of Naval Research Attn: Code 1113 800 N. Quincy Street Arlington, Virginia 22217-5000	2
Dr. Bernard Douda Naval Weapons Support Center Code 50C Crane, Indiana 47522-5050	1
Naval Civil Engineering Laboratory Attn: Dr. R. W. Drisko, Code L52 Port Hueneme, California 93401	1
Defense Technical Information Center Building 5, Cameron Station Alexandria, Virginia 22314	12 high quality
DTNSRDC Attn: Dr. H. Singerman Applied Chemistry Division Annapolis, Maryland 21401	1
Dr. William Tolles Superintendent Chemistry Division, Code 6100 Naval Research Laboratory Washington, D.C. 20375-5000	1
Dr. David Young Code 334 NORDA NSTL, Mississippi 39529	1
Naval Weapons Center Attn: Dr. Ron Atkins Chemistry Division China Lake, California 93555	1
Scientific Advisor Commandant of the Marine Corps Code RD-1 Washington, D.C. 20380	1
U.S. Army Research Office Attn: CRD-AA-IP P.O. Box 12211 Research Triangle Park, NC 27709	1
Mr. John Boyle Materials Branch Naval Ship Engineering Center Philadelphia, Pennsylvania 19112	1
Naval Ocean Systems Center Attn: Dr. S. Yamamoto Marine Sciences Division San Diego, California 91232	1

DL/1113/87/2

ABSTRACTS DISTRIBUTION LIST,359/627

Dr. Manfred Breiter
Institut fur Technische Elektrochemie
Technischen Universitat Wien
9 Getreidemarkt, 1160 Wien
AUSTRIA

Dr. E. Yeager
Department of Chemistry
Case Western Reserve University
Cleveland, Ohio 44106

Dr. R. Sutula
The Electrochemistry Branch
Naval Surface Weapons Center
Silver Spring, Maryland 20910

Dr. R. A. Marcus
Department of Chemistry
California Institute of Technology
Pasadena, California 91125

Dr. J. J. Auborn
AT&T Bell Laboratories
600 Mountain Avenue
Murray Hill, New Jersey 07974

Dr. M. S. Wrighton
Chemistry Department
Massachusetts Institute
of Technology
Cambridge, Massachusetts 02139

Dr. B. Stanley Pons
Department of Chemistry
University of Utah
Salt Lake City, Utah 84112

Dr. Bernard Spielvogel
U.S. Army Research Office
P.O. Box 12211
Research Triangle Park, NC 27709

Dr. Mel Miles
Code 3852
Naval Weapons Center
China Lake, California 93555

Dr. P. P. Schmidt
Department of Chemistry
Oakland University
Rochester, Michigan 48063

Dr. Roger Belt
Litton Industries Inc.
Airtron Division
Morris Plains, NJ 07950

Dr. Ulrich Stimming
Department of Chemical Engineering
Columbia University
New York, NY 10027

Dr. Royce W. Murray
Department of Chemistry
University of North Carolina
Chapel Hill, North Carolina 27514

Dr. Michael J. Weaver
Department of Chemistry
Purdue University
West Lafayette, Indiana 47907

Dr. R. David Rauh
EIC Laboratories, Inc.
Norwood, Massachusetts 02062

Dr. Edward M. Eyring
Department of Chemistry
University of Utah
Salt Lake City, UT 84112

Dr. M. M. Nicholson
Electronics Research Center
Rockwell International
3370 Miraloma Avenue
Anaheim, California

Dr. Nathan Lewis
Department of Chemistry
Stanford University
Stanford, California 94305

Dr. Hector D. Abruna
Department of Chemistry
Cornell University
Ithaca, New York 14853

Dr. A. B. P. Lever
Chemistry Department
York University
Downsview, Ontario M3J 1P3

DL/1113/87/2

ABSTRACTS DISTRIBUTION LIST, 359/627

Dr. Martin Fleischmann
Department of Chemistry
University of Southampton
Southampton SO9 5H UNITED KINGDOM

Dr. John Wilkes
Department of the Air Force
United States Air Force Academy
Colorado Springs, Colorado 80840-6528

Dr. R. A. Osteryoung
Department of Chemistry
State University of New York
Buffalo, New York 14214

Dr. Janet Osteryoung
Department of Chemistry
State University of New York
Buffalo, New York 14214

Dr. A. J. Bard
Department of Chemistry
University of Texas
Austin, Texas 78712

Dr. Steven Greenbaum
Department of Physics and Astronomy
Hunter College
695 Park Avenue
New York, New York 10021

Dr. Donald Sandstrom
Boeing Aerospace Co.
P.O. Box 3999
Seattle, Washington 98124

Mr. James R. Moden
Naval Underwater Systems Center
Code 3632
Newport, Rhode Island 02840

Dr. D. Rolison
Naval Research Laboratory
Code 6171
Washington, D.C. 20375-5000

Dr. D. F. Shriver
Department of Chemistry
Northwestern University
Evanston, Illinois 60201

Dr. Alan Bewick
Department of Chemistry
The University of Southampton
Southampton, SO9 5NH UNITED KINGDOM

Dr. Edward Fletcher
Department of Mechanical Engineering
University of Minnesota
Minneapolis, Minnesota 55455

Dr. Bruce Dunn
Department of Engineering &
Applied Science
University of California
Los Angeles, California 90024

Dr. Elton Cairns
Energy & Environment Division
Lawrence Berkeley Laboratory
University of California
Berkeley, California 94720

Dr. Richard Pollard
Department of Chemical Engineering
University of Houston
Houston, Texas 77004

Dr. M. Philpott
IBM Research Division
Mail Stop K 33/801
San Jose, California 95130-6099

Dr. Martha Greenblatt
Department of Chemistry, P.O. Box 939
Rutgers University
Piscataway, New Jersey 08855-0939

Dr. Anthony Sammells
Eltron Research Inc.
4260 Westbrook Drive, Suite 111
Aurora, Illinois 60505

Dr. C. A. Angell
Department of Chemistry
Purdue University
West Lafayette, Indiana 47907

Dr. Thomas Davis
Polymers Division
National Bureau of Standards
Gaithersburg, Maryland 20899

DL/1113/87/2

ABSTRACTS DISTRIBUTION LIST, 359/627

Dr. Stanislaw Szpak
Naval Ocean Systems Center
Code 633, Bayside
San Diego, California 95152

Dr. Gregory Farrington
Department of Materials Science
and Engineering
University of Pennsylvania
Philadelphia, Pennsylvania 19104

Dr. John Fontanella
Department of Physics
U.S. Naval Academy
Annapolis, Maryland 21402-5062

Dr. Micha Tomkiewicz
Department of Physics
Brooklyn College
Brooklyn, New York 11210

Dr. Lesser Blum
Department of Physics
University of Puerto Rico
Rio Piedras, Puerto Rico 00931

Dr. Joseph Gordon, II
IBM Corporation
5600 Cottle Road
San Jose, California 95193

Dr. Joel Harris
Department of Chemistry
University of Utah
Salt Lake City, Utah 84112

Dr. J. O. Thomas
University of Uppsala
Institute of Chemistry
~~Box 531 Baltimore, Maryland 21218~~
S-751 21 Uppsala, Sweden

Dr. John Owen
Department of Chemistry and
Applied Chemistry
University of Salford
Salford M5 4WT UNITED KINGDOM

Dr. O. Stafsudd
Department of Electrical Engineering
University of California
Los Angeles, California 90024

Dr. Boone Owens
Department of Chemical Engineering
and Materials Science
University of Minnesota
Minneapolis, Minnesota 55455

Dr. Johann A. Joebstl
USA Mobility Equipment R&D Command
DRDME-EC
Fort Belvoir, Virginia 22060

Dr. Albert R. Landgrebe
U.S. Department of Energy
M.S. 6B025 Forrestal Building
Washington, D.C. 20595

Dr. J. J. Brophy
Department of Physics
University of Utah
Salt Lake City, Utah 84112

Dr. Charles Martin
Department of Chemistry
Texas A&M University
College Station, Texas 77843

Dr. Milos Novotny
Department of Chemistry
Indiana University
Bloomington, Indiana 47405

Dr. Mark A. McHugh
Department of Chemical Engineering
The Johns Hopkins University
Baltimore, Maryland 21218

Dr. D. E. Irish
Department of Chemistry
University of Waterloo
Waterloo, Ontario, Canada
N21 3G1

DL/1113/87/2

ABSTRACTS DISTRIBUTION LIST, 359/627

Dr. Henry S. White
Department of Chemical Engineering
and Materials Science
151 Amundson Hall
421 Washington Avenue, S.E.
Minneapolis, Minnesota 55455

Dr. Daniel A. Buttry
Department of Chemistry
University of Wyoming
Laramie, Wyoming 82071

Dr. W. R. Fawcett
Department of Chemistry
University of California
Davis, California 95616

Dr. Peter M. Blonsky
Eveready Battery Company, Inc.
25225 Detroit Road, P.O. Box 45035
Westlake, Ohio 44145